RESEARCH PAPER

# Corrosion and Antibacterial Behavior of CrN Single-layer Coating and CrN/Cu Multilayer Nanostructured Coatings Applied by Cathodic Arc Evaporation Technique

**Mozhgan Hirbodjavan, Arash Fattah-alhosseini*, Hassan Elmkhah, Omid Imantalab**

* *a.fattah@basu.ac.ir*

Department of Materials Engineering, Bu-Ali Sina University, Hamedan, 65178-38695, Iran

**Received: December 2021** **Revised: September 2022** **Accepted: October 2022**
***DOI: 10.22068/ijmse.2615***

***Abstract:*** *The principal goal of this research is to produce a CrN/Cu multilayer coating and a CrN single-layer coating and also compare their electrochemical and antibacterial behavior. In this investigation, the coatings were applied to the stainless steel substrate by cathodic arc evaporation a sub-division of physical vapor deposition (CAE-PVD). The present phases were characterized and the thickness of the coatings was measured using X-ray diffraction (XRD) and field emission scanning electron microscopy (FE-SEM), respectively. Rockwell-C tester was used to evaluate the adhesion quality. Also, to evaluate the mechanical properties of the coatings such as modulus of elasticity and hardness, a nanoindentation test was used and the indentation effect and coating topography were evaluated using atomic force microscopy (AFM). Studying the electrochemical behavior of the coatings was done using electrochemical impedance spectroscopy (EIS) and potentiodynamic polarization (PDP) tests in Ringer's solution. The results of EIS tests showed that the CrN coating had higher polarization resistance in comparison to the CrN/Cu coating and an increasing trend of polarization resistance related to both coatings was identified by rising the time of immersion. Also, using the PDP curves, the CrN and CrN/Cu coating current densities were estimated at $1.835\times10^{-8}$ and $2.088\times10^{-8}$, respectively. The antibacterial activity of CrN and CrN/Cu coatings was evaluated by the spot-inoculation method. The results of the antibacterial test indicated that compared to CrN coating, CrN/Cu coating had a better impact on the control of the bacteria growth.*

***Keywords:*** *multilayer nanostructured coating, CrN/Cu, CAE-PVD, electrochemical impedance spectroscopy (EIS), antibacterial behavior.*

## 1. INTRODUCTION

Stainless steel is one of the most common materials in the manufacture of medical tools [1]. These materials have remarkable properties such as biocompatibility, high strength, and mechanical stability [2, 3]. However, the main problem with these materials is their unpleased tribological properties and corrosion resistance that are significant for medical applications and due to this, a lot of research has been carried out to remove these unpleasant properties [4]. Cavity corrosion can occur in stainless steel and the resistance to local corrosion of steel depends on the concentration of chloride in the environment [5]. The surface of a metal is the first site to come into contact with the environment. Thus, it specifies biological efficiency and performance [6]. Modification of the mechanical properties in the surface using transition metal nitrides is a famous method [7]. The surface properties of the material are of specific importance because the surface protects the main material and plays a major role in the lifetime of the part [8]. On the other hand, surface coatings on metals and alloys affect their corrosion behavior [9].

To achieve higher corrosion resistance, coatings with bilayer or multilayer architectures are currently utilized and perform better than single-layer coatings [10]. At present, different methods such as the sol-gel, hydrothermal procedure, pulsed laser deposition (PLD), chemical vapor deposition (CVD), physical vapor deposition (PVD), and magnetron sputtering are used to deposit the coatings on various surfaces. The most common technique to obtain thin hard coatings is the PVD method. PVD processes (commonly referred to as thin film procedures) are atomic deposition processes in which materials evaporate from a solid or liquid source in the form of an atom or molecule and are moved to the substrate. Generally, PVD procedures are used to deposit coatings in the range of a few nanometers to thousands of nanometers [11, 12].

Multilayer coatings based on transition metals, including titanium and chromium, improve surface properties. One of the most significant advantages of multilayer coatings is that each



[ DOI: 10.22068/ijmse.2615 ]

layer performs a particular function on the surface of the material [13]. The multilayer structure of the coating is considered an effective method to improve the hardness. Using this structure, the interfaces of the layers can divert cracks and provide barriers to dislocation [14]. Multilayer coatings, particularly those composed of transition metal nitrides have been considered by researchers because of their properties, usefulness, and special scientific importance [15, 16].

Metal nitride coatings of transition metals have been widely used in the industry owing to their exceptional physical and chemical properties such as high hardness, good wear resistance, and high-temperature stability in addition to oxidation and corrosion resistance [17, 18, 27, 19–26]. These materials are often used as an inhibitory protective coating on metal substrates to reduce corrosion. The purpose of inhibitory protective coating is to prevent the reaction of corrosive species with the metal surface in the corrosion environment [28]. In comparison to the TiN coating which appears to be the most popular intermetallic metal nitride, CrN coatings have better wear properties, higher thermal stability, and better corrosion resistance [7, 29–34]. Reported research on CrN coatings has focused mostly on oxidation and corrosion resistance [35]. In general, CrN coating as a hard coating has great properties that are widely used in the industry to protect the base material (substrate) against abrasive wear, fatigue wear, corrosion, and other surface damage. Ceramic coatings are hard and wear-resistant, however, they are considered brittle coatings. So, the hardness of these coatings can be improved by using metal layers between hard ceramic films [7]. In addition, elements such as silver or copper nanoparticles can give antibacterial properties to coatings [36, 37]. Stainless steel is one of the most common materials used in hygienic environments and many health-related devices, and having antibacterial capabilities increases its applications. In recent years, some researchers have suggested the use of Cu or Cu alloys as touching surfaces in hospitals to significantly reduce surface-related health problems [38]. Copper is used for clinical applications due to its low toxicity and high compatibility with the human body [39]. The properties of multilayer coatings that include antibacterial elements and transition metal nitrides are an interesting rubric that has not attracted much attention so far. Among PVD procedures, a cathodic arc is a common method to apply coating due to its excellent coating properties. High hardness, good adhesion to the substrate, high density, and homogeneity are the characteristics of coatings applied using this method and show better properties compared with coatings created by the magnetron sputtering method [27, 40–47]. Using the PVD method, a variety of coatings can be created, including pure metals, metal carbides, and metal nitrides [48]. The purpose of this study is to apply CrN/Cu multilayer coating using the PVD method from using cathodic arc and to investigate and compare its electrochemical and antibacterial behavior with CrN single-layer coating. Escherichia coli (E. coli) and Staphylococcus aureus (S. aureus) were selected as pathogens to evaluate antibacterial activity [49].

## 2. EXPERIMENTAL PROCEDURES

### 2.1. Coating deposition process

The coating was deposited on AISI 304 stainless steel substrates with dimensions of 2×40×40 mm. Before applying the coating, the substrates were cleaned in acetone and alcohol for 20 minutes using an ultrasonic bath. CrN/Cu multilayer and CrN single-layer coatings were applied using CAE-PVD (CA&MS601, Yar-Nikan Saleh, Iran). Deposition conditions are presented in Table 1.

### 2.2. Microstructural Analysis

The XRD (Philips pw1730) was used to characterize the phases associated with the coating using a Cu $K_\alpha$ beam with a wavelength of 1.54 angstroms. XRD patterns were recorded under a voltage of 40 kV in the diffraction angle range of 20 to 80 degrees with a step size of 0.05 and a step time of 1 second. XRD test peaks were identified using X'pert HighScore software. A JSM-84 SEM was used to observe the microstructure and surface morphology. Also, the cross-section of the coatings and the number of layers were observed using the FE-SEM device model MIRA3 TESCAN.

### 2.3. Evaluation of Mechanical Properties

To investigate the mechanical properties such as modulus of elasticity and hardness, a force of 5000 μN, and a 5 s load and 5 s unload (from five different points), a TriboScope nanoindentation device with a 2D converter and a Berkovich



[ DOI: 10.22068/ijmse.2615 ]

diamond indenter with an angle of 142.3 degrees was used.
To avoid the effects of substrate hardness on the mechanical properties of the coatings, the depth of the applied indentation was less than 10% of the thickness of the coating. The AFM NanoScope III digital device was used to observe the indentation effect and topography of the coating. According to the standard of VDI 3198 [50–53], the adhesion test was performed by a Rockwell-C macro-hardness device with a force of 1473 N and a time of 20 seconds, the effect of which was tested using an optical microscope.

### 2.4. Electrochemical Tests

Electrochemical tests, including EIS and PDP tests, were carried out by a potentiostat/galvanostat (μAutolab Type III/FRA2). Samples were cleaned with distilled water before the corrosion test. Before performing the PDP test, the samples were immersed in the solution for 168 hours under open-circuit potential (OCP) conditions. Then, the potential scan was performed from -250 mV relative to the OCP up to a potential of 1.2 V at a rate of 1 mV/s. It should be noted that all tests using the standard three-electrode tube, including the platinum electrode as a helping electrode, the silver/silver chloride electrode (Ag/AgCl) as the reference electrode, and the test specimen as the working electrode were performed in a Ringer environment. Also, EIS tests were performed in the frequency range of 100 kHz to 10 mHz and the sinusoidal excitation potential of 5 mV after 2, 24, 72, and 168 hours of immersion in OCP conditions on both coatings.
To ensure the confirmation of the results, each electrochemical test was repeated 5 times. In addition, Kramers-Kronig diagrams were used to confirm the experimental EIS measurements. Nova software was used to simulate EIS experimental data.

### 2.5. Antibacterial Test

The antibacterial behavior of CrN and CrN/Cu coatings was evaluated on S. aureus (gram-positive pathogenic bacteria) (ATCC 6538) and E. coli (gram-negative pathogenic bacteria) (ATCC 25922) by the spot-inoculation method. The adjusted bacterial suspensions (about $5 \times 10^5$ CFU/mL) by spectrophotometry (Pharmacia LKB-Nova Spacell, Cambridge, UK) were inoculated on the surface of sterilized coatings and then incubated for 3 hours at 35°C. Finally, the surviving bacterial cells were counted by culturing the samples on Müller-Hinton agar to measure the antibacterial effect of the coatings.

## 3. RESULTS AND DISCUSSION

### 3.1. Structural Analysis

Fig. 1 shows the morphology of the CrN and CrN/Cu coatings on the substrate of AISI 304 stainless steel. As can be seen, both images have macro-particles and pinholes. These macro-particles are droplets from molten cathodes in the PVD coating with the cathodic arc. It should be noted that the presence of macro-particles and pinholes is an inherent feature of coatings created by the PVD with the cathodic arc evaporation method that has been reported in other published scientific papers [47, 52].
The mentioned defects can be the passage of corrosive solution from the coating into the substrate that can block the path of the solution to the substrate and increase the corrosion resistance of the coating by creating multilayer coatings and closing the mentioned defects during the formation of the coating [47, 54]. It can be said that the created interfaces during the deposition of multilayer coatings have a dual role in corrosion resistance.

**Table 1.** Deposition parameters of the coatings

| Coating parameters | Cu | CrN |
|---|---|---|
| Target | 99.96% Cu | 99.96% Cr |
| Inlet gas | $N_2$ and Ar | $N_2$ and Ar |
| Working pressure (torr) | $5 \times 10^{-3}$ | $5 \times 10^{-3}$ |
| distance between target-substrate (cm) | 15 | 15 |
| Time deposition (min) | 105 | 105 |
| Rotation speed of parts (RPM) | 5 | 5 |
| Bias voltage (V) | -100 | -100 |
| Target evaporation current (A) | 120 | 120 |
| Deposition temperature (°C) | 200 | 200 |


[ DOI: 10.22068/ijmse.2615 ]

Although the interfaces can block the penetration of the corrosive solution into the substrate, the active presence of interfaces may raise the corrosion rate due to the possibility of galvanic corrosion between interfaces [48, 54].

Fig. 2 shows the FE-SEM images of the cross-section of the coatings. Fig. 2(a) shows a CrN coating with a thickness of 1.8 µm and Fig. 2(b and C) shows a CrN/Cu multilayer coating with two different magnifications which are 6 CrN-Cu pairs of layers and the last layer is a combination of CrN and Cu (CrCuN coating). Due to the difference in atomic numbers and its effect on the brightness of the images, the light layers are related to Cu and the dark layers are related to CrN. The thickness of the CrN layer is 0.5 µm and the Cu layer is 43 nm with an overall thickness of 3.6 µm. In addition, a pure Cr layer is observed between the coating and the substrate that is applied for better adhesion of the coating and the substrate [55].

Fig. 3 shows the XRD pattern for CrN/Cu multilayer and CrN single-layer coatings on AISI 304 stainless steel substrates. According to this figure, the CrN peaks of both coatings are approximately at the same diffraction angle. The crystal structure of both is the same as each other and has a NaCl structure (type B1).

In the XRD pattern of the CrN coating, due to the approximate thickness of 2 microns of the coating (shown in Fig. 2), peaks of the interlayer of Cr and $\gamma_{Fe}$ (substrate) are also observed. In CrN/Cu coating, Cu (111) peak overlaps with the CrN (002) peak.

Fig. 4 illustrates optical microscope images of the indentation effect of Rockwell-C. According to VDI 3198 standard, the observed image is in accordance with the HF1 class that shows the appropriate quality in adhesion of the coating to the substrate [51].

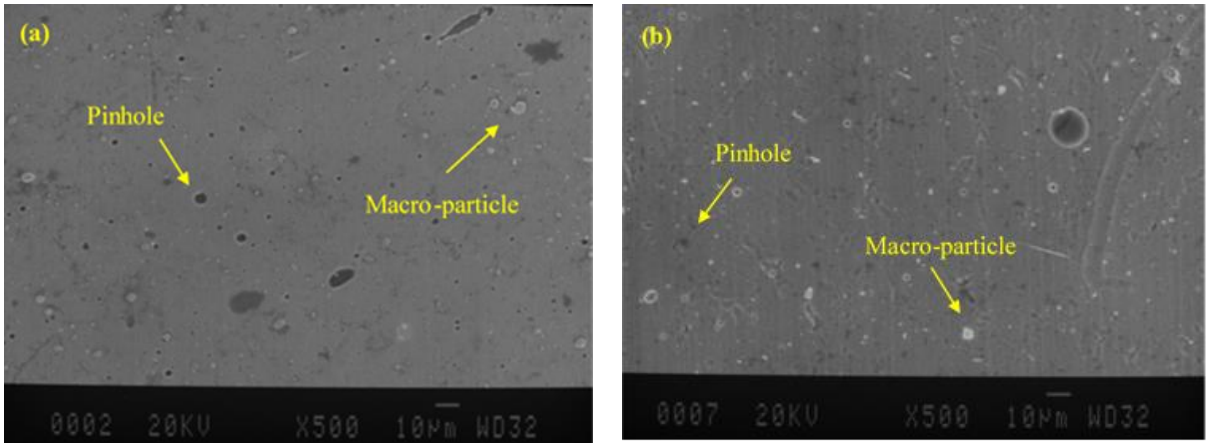


**Fig. 1.** Images of SEM for surface morphology: (a) CrN coating and (b) CrN/Cu coating.

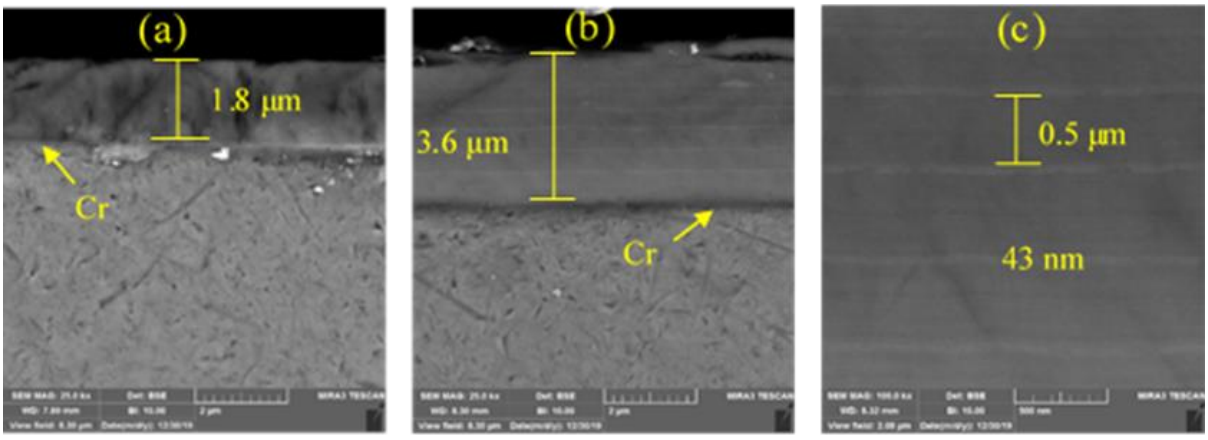


**Fig. 2.** FE-SEM images of the cross-section of the coatings (a) CrN single-layer coating (b) CrN/Cu multilayer coating, (c) CrN/Cu multilayer coating with higher magnification.





[ DOI: 10.22068/ijmse.2615 ]

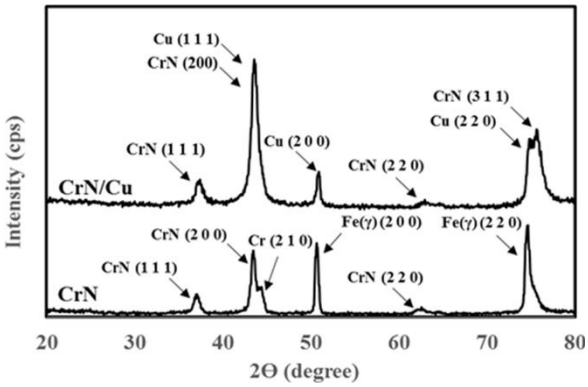


**Fig. 3.** XRD pattern for CrN and CrN/Cu coatings.

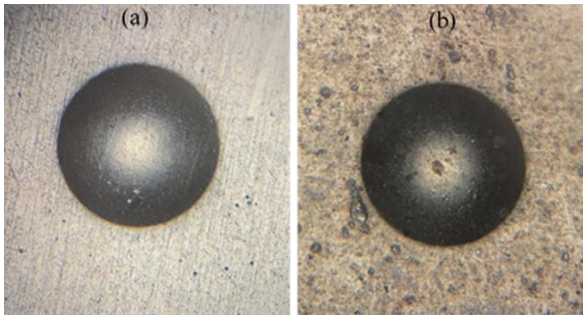


**Fig. 4.** Optic microscope images of the indentation effect of Rockwell-C for the adhesion evaluation: (a) CrN, and (b) CrN/Cu.

### 3.2. Studying the Mechanical Properties

As shown in Fig. 5, the amount of displacement in the CrN coating is less than that of the CrN/Cu coating by the same force which indicates that the CrN coating is more resistant against deformation in comparison to the CrN/Cu coating. Table 2 indicates the average H values for the coatings. The existence of copper metal in the multilayer coating and its softness causes a reduction in the hardness value [56–58].

Table 2 indicates the values of H/E* and the $H^3/E^{*2}$ values. The value of H/E* is the indicator of the elastic behavior of the surface in contact with external forces. The value of $H^3/E^{*2}$ is also an indicator of the evaluation of plastic deformation resistance [59–61]. In addition to the chemical composition and microstructure of the coating, the properties of the deposited coating are also affected by the morphology of the coating surface [7].

Fig. 6 shows AFM images before and after the nanoindentation test of both coatings. As shown in Fig. 6, the depth of the indenter in the CrN coating is less than that of the CrN/Cu coating due to its higher hardness. According to the reported roughness values in Table 3, it is clear that the roughness of the CrN/Cu coating is lower in comparison to the CrN coating.

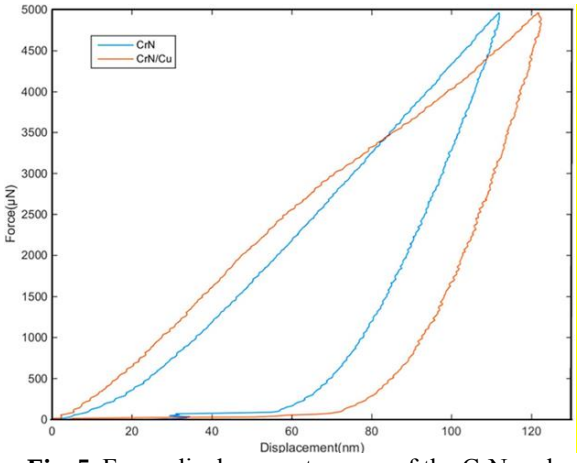


**Fig. 5.** Force-displacement carves of the CrN and CrN/Cu coatings.

**Table 2.** The mechanical evaluation values of the CrN and CrN/Cu coatings obtained from nanoindentation response

| Sample | H(GPa) | Er(GPa) | $H^3/E^{*2}$ | H/E* |
|---|---|---|---|---|
| CrN | 19.5± 2.1 | 2485± 18 | 0.119 | 0.078 |
| CrN/Cu | 16.1± 0.84 | 2867±3 | 0.050 | 0.056 |

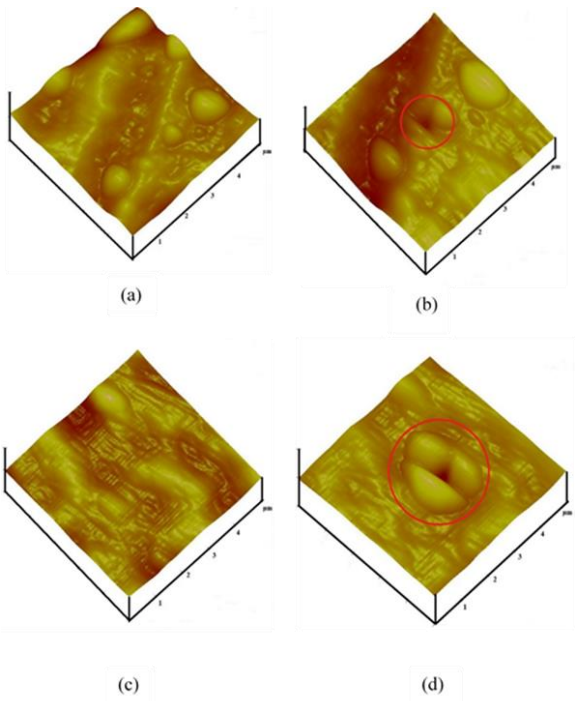


**Fig. 6.** AFM images: (a) before nanoindentation in CrN coating, (b) after nanoindentation in CrN coating, (c) before nanoindentation in CrN/Cu coating and (d) after nanoindentation in CrN/Cu coating.



[ DOI: 10.22068/ijmse.2615 ]

**Table 3.** Values of roughness for CrN and CrN/Cu coatings

| Sample | $R_a$ (nm) | $R_z$ (nm) | RMS (nm) |
|---|---|---|---|
| CrN | 13.8 | 135.9 | 17.2 |
| CrN/Cu | 6.3 | 50.3 | 7.9 |

### 3.3. Studying the Electrochemical Behavior

Fig. 7 shows the changes in OCP in terms of immersion time in the Ringer medium for both CrN and CrN/Cu coatings. As illustrated in this figure, the CrN coating curve shows more noble potential values in comparison to the CrN/Cu coating curve. This behavior indicates that the thermodynamic tendency is less to start the corrosion process related to the CrN coating. According to Fig. 7, passing time, the immersion potential values of both open circuits for both coatings first decrease and then increase. Also, after an approximate time of 1800 seconds, the OCP changes related to both coatings are little and both coatings have reached proper stability [7]. The change of OCP to negative or more active values can be owing to the adsorption of chloride anions, the change in the concentration of metal ions, the change in surface activity or penetration of the electrolyte into the coating or dissolution of metal oxides in the surface of the sample. On the other hand, the rise in OCP over time can be due to the formation of a surface oxide film [62].

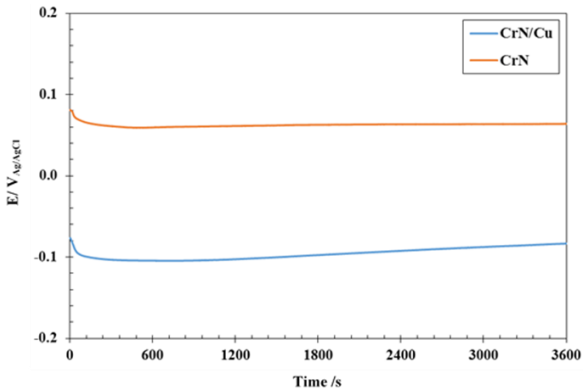


**Fig. 7.** OCP plot for CrN and CrN/Cu coatings in Ringer's solution

The PDP curve of the investigated samples after 3 days of immersion in Ringer's solution is illustrated in Fig. 8. According to Fig. 8, both coatings formed in Ringer's solution have shown passive behavior. PDP curves that are similar to this study have been reported concerning the created CrN coating by the PVD using cathodic arc at 3.5% of sodium chloride [63]. In addition, studying the effect of immersion time on the electrochemical behavior of CrN coating has indicated that the corrosion current density decreases by rising immersion time in the medium of 3.5% of sodium chloride [63].

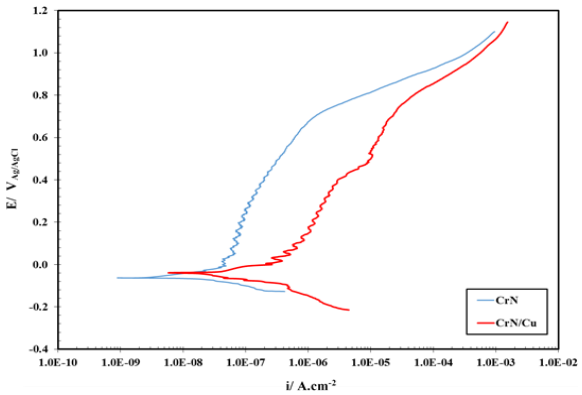


**Fig. 8.** PDP curves for CrN and CrN/Cu coatings applied on stainless steel substrates.

The values of corrosion potential and current density (using the Tafel method) for both specimens are summarized in Table 4. The corrosion current density (icorr) was obtained from PDP plots using the method of Tafel linear extrapolation [63].

**Table 4.** Values of corrosion current and corrosion potential from PDP plots

| Sample | $i_{corr}$ (A.cm$^{-2}$) | $E_{corr}$ (V) |
|---|---|---|
| CrN | $1.835 \times 10^{-8}$ | -0.0628 |
| CrN/Cu | $2.08 \times 10^{-8}$ | -0.0387 |

Based on the reported data in Table 4, CrN coating shows higher corrosion potential and lower current density in comparison to CrN/Cu coating which indicates higher corrosion resistance of CrN coating. It is known that the transition of metal nitrides is neutral against chemical attacks owing to their relatively high potential in the electrochemical series table and so, shows high thermodynamic resistance against the commencement of corrosion [7]. Also, CrN coating can form a surface layer with dense microstructure [64, 65]. To compare and investigate the effect of time on the electrochemical behavior of two coatings, the EIS test was used as a non-destructive, fast, and powerful approach [66, 67].

Fig. 9 shows the results of the EIS test for both CrN and CrN/Cu coatings after different immersion times in the Ringer solution (under



[ DOI: 10.22068/ijmse.2615 ]

OCP conditions) in the form of Nyquist and Bode curves. Considering that the general shape of EIS diagrams related to both coatings in both Nyquist and Bode curves is the same by rising immersion time, it can be said that the mechanism of the electrochemical behavior of both coatings has not changed by rising the immersion time. Nyquist curves are drawn from real data in terms of imaginary data. According to the Nyquist curves shown in Fig. 9, the diameters of the capacitive rings for both samples show an increasing trend with increasing immersion time. This behavior indicates that the anti-corrosion behavior of both coatings, which is inversely related to the corrosion rate, improves with increasing time. Also, based on the Nyquist diagrams presented in Fig. 9, it can be said that increasing the immersion time from 2 hours to 168 hours had a significant effect on the polarization resistance of the CrN/Cu coating. In Nyquist diagrams, the diameter of capacitive rings indicates polarization resistance.

In the Bode curves indicated in Fig. 9(c and d), the phase changes in terms of frequency (Bode-phase) and the changes in the total amount of impedance in terms of frequency (Bode-modulus) are plotted. In the Bode-phase diagram, the maximum value of the coating angle for both coatings is less than 90 degrees which shows a deviation from the ideal capacitor [68]. Also, the existence of two-time constants in the Bode diagrams presented in Fig. 9 is visible for both coatings. Thus, it is vital to use an equivalent electrical circuit consisting of two-time constants to simulate the EIS data. The data of EIS are valid when they meet the limitations of linear system theory, such as causality, linearity, and stability [69]. For this aim, Kramers-Kronig curves are used to check the validity of experimental data. Kramers-Kronig transformations are gained by converting the real axis to an imaginary axis and vice versa.

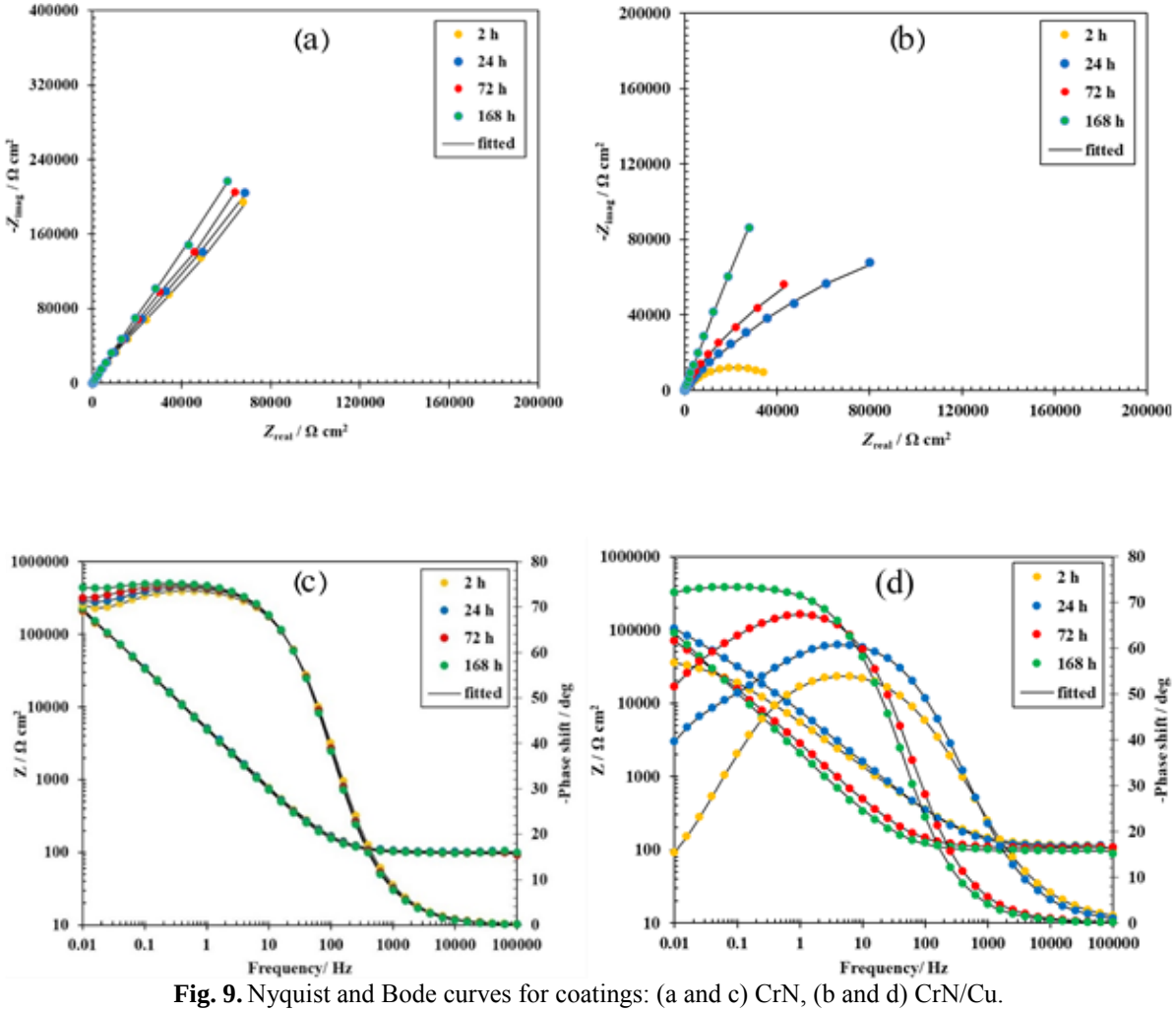


**Fig. 9.** Nyquist and Bode curves for coatings: (a and c) CrN, (b and d) CrN/Cu.



[ DOI: 10.22068/ijmse.2615 ]

The transform equations of Kramers-Kronig are expressed by Equations 1 and 2 [70]:

$$Z_{Re}(\omega) = \frac{2}{\pi} \cdot \int_0^{\infty} \frac{\omega' . Z_{Im}(\omega')}{\omega^2 - \omega'^2} d\omega' \quad (1)$$

$$Z_{Im}(\omega) = \frac{-2}{\pi} \cdot \int_0^{\infty} \frac{\omega . Z_{Re}(\omega')}{\omega^2 - \omega'^2} d\omega' \quad (2)$$

In Fig. 10, the diagrams of Kramers-Kronig together with the EIS experimental data are reported to both coatings after 7 hours in Ringer's solution. Appropriate overlap of experimental data with Kramers-Kronig data shows that the electrochemical system is stable during the test and the results are valid [70, 71]. This overlap was present in the other examined durations that were skipped in this part.

The electrical equivalent circuit shown in Fig. 11 was used to simulate the results of EIS. In this equivalent circuit, $R_s$ is the soluble resistance between the coating surface and the reference electrode, $R_1$ is the coating resistance, $Q_1$ is the coating constant phase element (CPE), $R_2$ is the charge transfer resistance, and $Q_2$ is the time constant related to the electrical double layer.

In other published scientific sources [7, 24] from the same equivalent electrical circuit indicated in Fig. 11 was used to simulate the experimental EIS data associated with single-layer and multilayer coatings. The impedance of the constant phase element is specified by Equation 3 [62, 72–77]:

$$Z_{CPE} = \frac{1}{Q(j\omega)^n} \quad (3)$$

Where Q is a frequency-independent parameter, j represents an imaginary unit, ω is an angular frequency, and n is a frequency-independent parameter ascribed to the deviation from the capacity of the ideal capacitor when n= 1, Q is equivalent to an ideal capacitor. Surface conditions and oxide layer performance can affect the value of n [72, 78, 79]. The emergence of a CPE behavior could be ascribed to many well-known factors such as the preferential active sites (i.e. impurities and grain boundaries), the existence of pores in the surface oxide films, and different types of surface heterogeneity on working electrodes (such as scratches, adsorption of ions, roughness and the impact of resistive variations that pertains to the covering passive films) [72, 78]. The obtained electrical parameters by the used equivalent electrical circuit are summarized in Table 5.

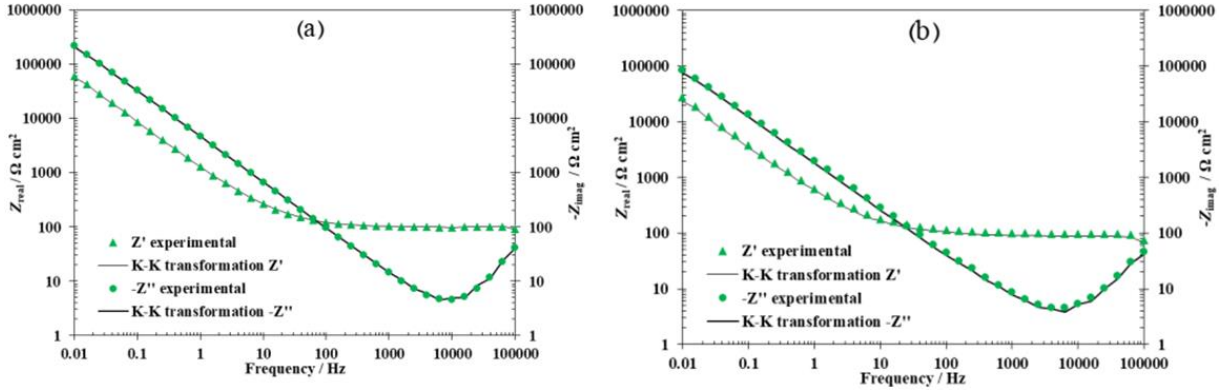


**Fig. 10.** Kramers-Kronig curves of (a) CrN and (b) CrN/Cu coatings.

**Table 5.** Extracted data from the proposed equivalent circuit

| sample | Immersion time (h) | $R_s$ ($\Omega.cm^2$) | $R_1$ ($\times 10^6$ $\Omega.cm^2$) | $Q_1$ ($\times 10^{-6}$ $S^{\alpha}.\Omega^{-1}.cm^{-2}$) | $n_1$ | $R_2$ ($\times 10^6$ $\Omega.cm^2$) | $Q_2$ ($\times 10^{-6}$ $S^{\alpha}.\Omega^{-1}.cm^{-2}$) | $n_2$ | $R_p$ ($\times 10^6$ $\Omega.cm^2$) |
|---|---|---|---|---|---|---|---|---|---|
| CrN | 2 | 101.53 | 0.08 | 42.25 | 0.84 | 5.86 | 15.77 | 0.89 | 6.70 |
| | 24 | 99.40 | 0.10 | 42.11 | 0.83 | 8.17 | 1.99 | 0.92 | 8.27 |
| | 72 | 96.56 | 0.15 | 43.85 | 0.84 | 14.58 | 11.63 | 0.91 | 14.73 |
| | 168 | 102.44 | 0.27 | 43.80 | 0.84 | 20.66 | 5.010 | 0.93 | 20.93 |
| CrN/Cu | 2 | 102.24 | 0.01 | 36.44 | 0.73 | 0.03 | 56.10 | 0.61 | 0.04 |
| | 24 | 104.37 | 0.06 | 29.74 | 0.72 | 0.22 | 32.96 | 0.65 | 0.28 |
| | 72 | 105.10 | 0.04 | 23.68 | 0.71 | 0.33 | 28.87 | 0.63 | 0.37 |
| | 168 | 97.90 | 0.61 | 21.22 | 0.73 | 5.62 | 13.50 | 0.63 | 6.22 |



[ DOI: 10.22068/ijmse.2615 ]

According to the data in Table 5, the polarization resistance ($R_p$= $R_1$ + $R_2$) of the CrN coating is higher than that of the CrN/Cu coating at any given immersion time. In addition, the data in Table 5 shows that the polarization resistance of both coatings increases over time. In addition, the significant effect of time on the polarization resistance of the CrN/Cu coating is clear, so after the immersion time from 2 h to 168 h, the polarization resistance of the coating has been changed from 0.0033 ($\times 10^6$ $\Omega.cm^2$) to 0.0031 ($\times 10^6$ $\Omega.cm^2$). While for CrN coating, the polarization resistance increased from 0.0021 ($\times 10^6$ $\Omega.cm^2$) to 0.0031 ($\times 10^6$ $\Omega.cm^2$).

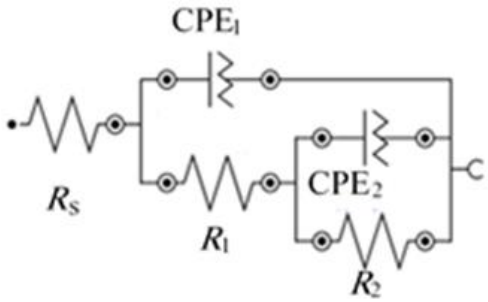


**Fig. 11.** Equivalent circuit to simulate EIS experimental data.

SEM images of the sample's surface after the PDP test for CrN single-layer and CrN/Cu multilayer coating are illustrated in Fig. 12. The general trend of coating/substrate corrosion is related to the destructive effect of macroparticles and cavities on PVD coatings [80]. Electrochemical experiments and surface analysis show that the main corrosion reactions of coatings are due to defects (pores, cavities, and cracks), coating delamination, and the galvanic effect between the drop and the coating [7]. Defects in the coating, such as cavities, form the route between the corrosive medium and the substrate. As can be seen in Fig. 12, these cavities cause the coating to be a cathode and anodize the substrate, and galvanic corrosion occurs. Also, the microparticles in the coating can be separated from the surface and cause pores in the coating. These pores can provide direct passage of corrosive solution and create pits. According to Fig. 12, more corrosion has occurred in the CrN/Cu coating which is consistent with Ref. [81]. The reason could be the existence of copper metal in the last layer.

### 3.4. Antibacterial Assay

The antibacterial potential of CrN and CrN/Cu coatings was assessed on E. coli and S. aureus. These bacteria are the most common pathogens that cause disease in humans and are used as the test bacteria in antimicrobial susceptibility assay [82, 83]. The results showed that E. coli count on CrN and CrN/Cu coatings was reached from 5.25 and 5.27 log CFU/mL to 4.8 and 4.5 log CFU/mL after 3 hours incubation, respectively. The control sample was uncoated and the bacteria behavior was examined in absence of inhibitory compounds to compare with the coated samples. E. coli population in the sample control increased from 5.24 to 5.64 log CFU/mL after 3 hours of inoculation (Fig. 13).

The antibacterial effect of the coatings on S. aureus was indicated that the surviving bacteria number on CrN and CrN/Cu coatings at the beginning hour inoculation was 5.28 and 5.26 log CFU/mL that reduced to 4.58 and 3.96 log CFU/mL after 3 hours inoculation, respectively.

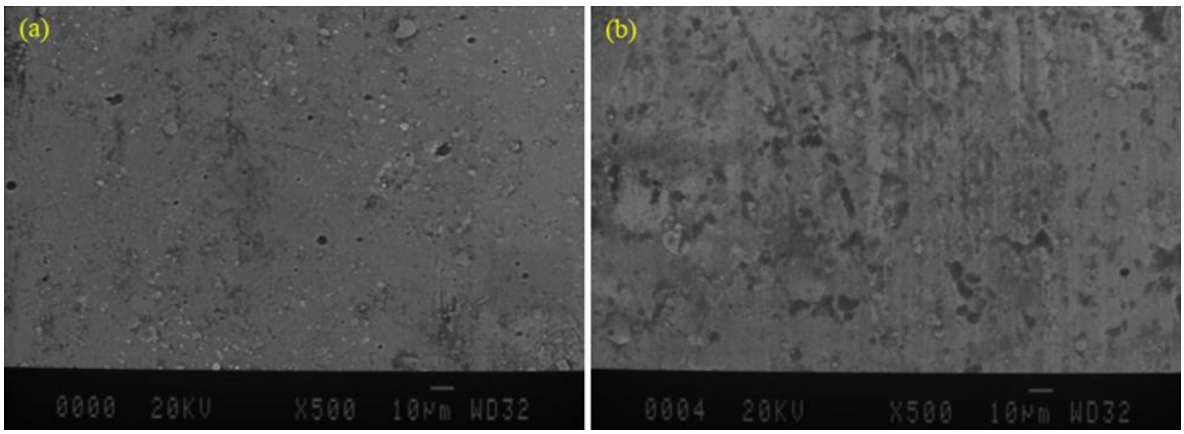


**Fig. 12.** Surface images of the coating after PDP measurement: (a) CrN single-layer coating, (b) CrN/Cu multilayer coating obtained from scanning electron microscopy.



[ DOI: 10.22068/ijmse.2615 ]

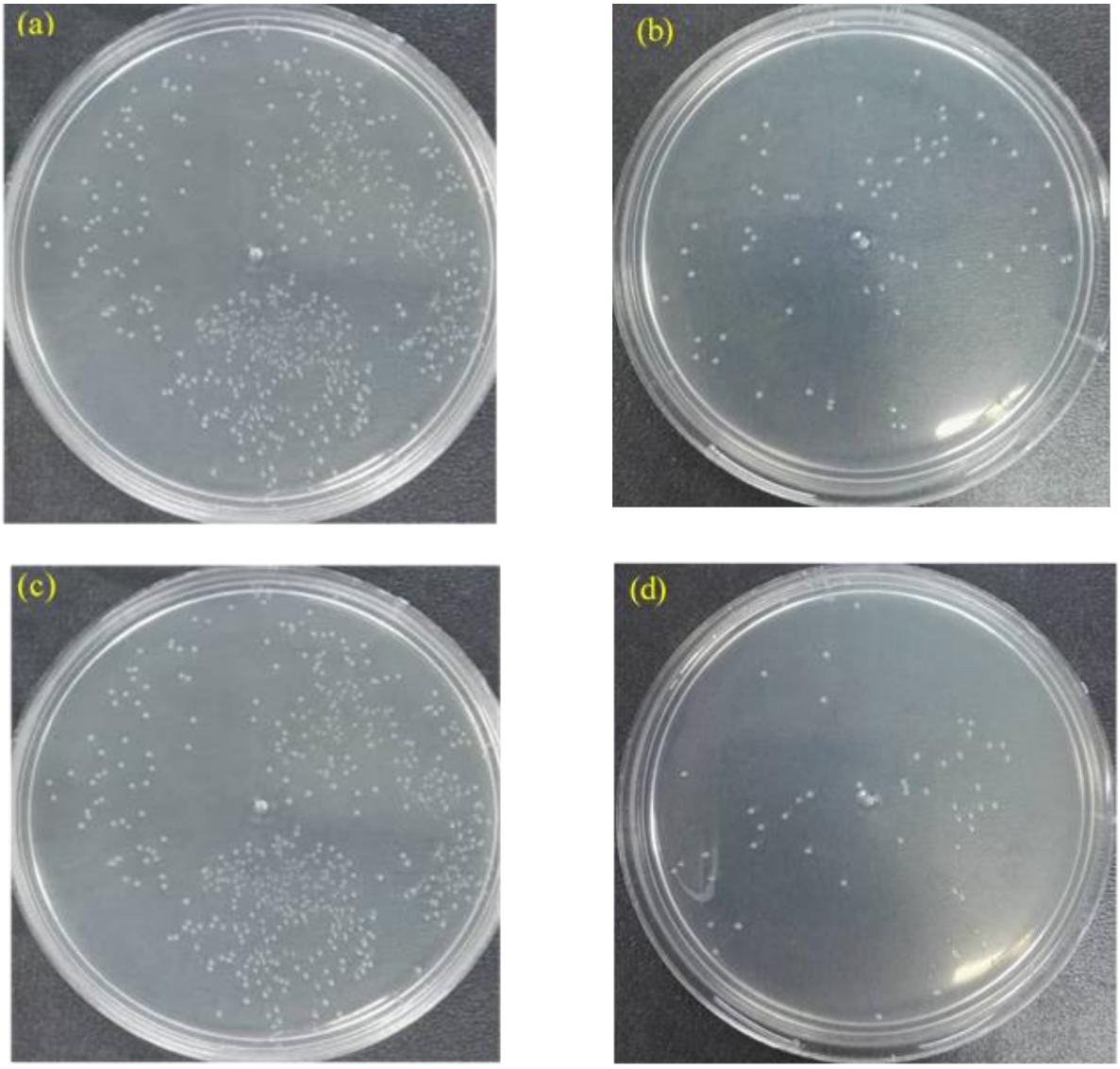


**Fig. 13.** The plate images of *E. coli*: the surviving cells from CrN and CrN/Cu coatings at zero hour (a and c) and after 3 hours inoculation (b and d) on Muller Hinton agar, respectively.

However, the S. aureus count in the control sample not only did not decrease but also increased, like E. coli (rose from 5.3 to 5.9 CFU/mL) (Fig. 14). According to the obtained data and performed experiments on E. coli and S. aureus, it was observed that the CrN/Cu coating had a greater antibacterial effect in comparison to the CrN coating owing to the existence of copper nanoparticles. Copper is a metal that has antibacterial properties and its existence in the coating rises the antibacterial effect. The main mechanism by which copper ions show antibacterial properties is binding and penetrating the bacterial cell wall [84].

$Cu^{2+}$ ions can extract electrons from bacteria, resulting in the production of reactive oxygen species (ROS) on the surface of the coating. In addition, ROS is converted to hydroxyl (HO) radicals that act as a deadly agent that hurts the bacterial cell wall [4]. Based on the results, it was realized that the rate of loss in S. aureus is higher than E. coli which can be owing to the bacterial form. Because S. aureus is clustered and E. coli is rod-shaped, S. aureus is more susceptible to degradation through bacterial walls owing to its higher contact surface with copper. Based on the results, it was realized that the decline rate of S. aureus was higher than E.coli on the coatings, which can be due to the spherical shape and the wall structural properties of S. aureus such as gram-positive and more susceptibility of the bacterial wall.





[ DOI: 10.22068/ijmse.2615 ]

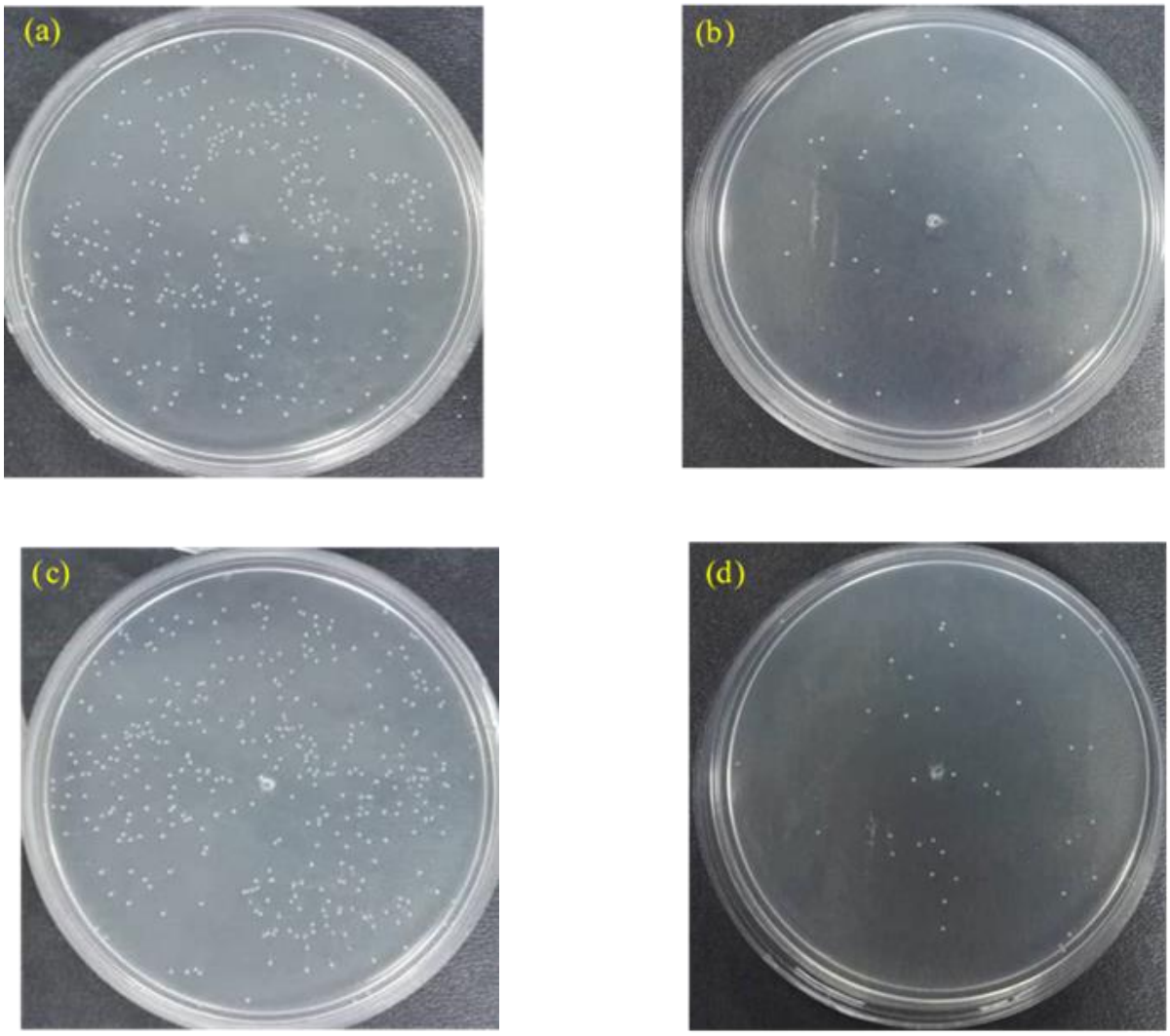


**Fig. 14.** The plate images of *S. aureus*: the surviving cells from CrN and CrN/Cu coatings at zero hour (a and c) and after 3 hours inoculation (b and d) on Muller Hinton agar, respectively.

## 4. CONCLUSIONS

In this research, CrN single-layer coating and CrN/Cu multilayer nanostructured coating were successfully applied on the substrate of AISI 304 stainless steel using by CAE-PVD method. By studying the mechanical, electrochemical, and antibacterial behavior of the coatings, the conclusion can be explained as follows:

1. SEM images showed that in both CrN and CrN/Cu coatings there are pinholes and macro-particles from the melted cathode in the method of CAE-PVD as inherent defects of this deposition method. By using FE-SEM images, the adhesion and the lack of any lamination effects of the coatings were specified.
2. The obtained results from the nanoindentation test showed that the hardness and elastic modulus of CrN and CrN/Cu coatings were 19.5 ± 2.1, 248 ± 18, 16.1 ± 0.84, and 287 ± 3 GPa. The reason for the low hardness of the CrN/Cu coating is the presence of soft copper metal. The obtained average roughness values were 13.8 nm for CrN coating and 6.3 nm for CrN/Cu coating. In addition, using the adhesion test, the adhesion of both coatings related to the desired substrate was assessed.
3. The obtained results from electrochemical measurements showed that over time, the polarization resistance of both coatings in the Ringer solution was improved. The corrosion current density of the CrN/Cu coating was more than CrN coating. Also, at any given



[ DOI: 10.22068/ijmse.2615 ]

immersion time, the CrN coating exhibited greater polarization resistance in comparison to the CrN/Cu coating.

4. Studying the antibacterial behavior of CrN and CrN/Cu coatings for E. coli and S. aureus showed that both coatings have antibacterial properties and the CrN/Cu coating compared to the CrN coating reduces the bacterial number even more after 3 hours owing to the presence of copper.

## REFERENCES


[1] Zalnezhad, E., Hamouda, A. M. S., Faraji, G., and Shamshirband, S., "$TiO_2$ nanotube coating on stainless steel 304 for biomedical applications", Ceram. Int., 2015, 41, 2785–2793.

[2] Wang, X., Yang, Z., Wang, Z., Shi, Q., Xu, B., Zhou, C., and Zhang, L., "The influence of copper on the stress corrosion cracking of 304 stainless steel", Appl. Surf. Sci., 2019, 478, 492–498.

[3] Lei, Z., Zhang, Q., Zhu, X., Ma, D., Ma, F., Song, Z., and Fu, Y. Q., "Corrosion performance of ZrN/$ZrO_2$ multilayer coatings deposited on 304 stainless steel using multi-arc ion plating", Appl. Surf. Sci., 2018, 431, 170–176.

[4] Kumar, D. D. and Kaliaraj, G. S., "Multifunctional zirconium nitride/copper multilayer coatings on medical grade 316L SS and titanium substrates for biomedical applications", J. Mech. Behav. Biomed. Mater., 2018, 77, 106–115.

[5] Lins, V. de F. C., Gonçalves, G. A. dos S., Leão, T. P., Soares, R. B., Costa, C. G. F., and Viana, A. K. do N., "Corrosion resistance of AISI 304 and 444 stainless steel pipes in sanitizing solutions of clean-in-place process", Mater. Res., 2016, 19, 333–338.

[6] Khalili, E. and Sarafbidabad, M., "Combination of laser patterning and nano PTFE sputtering for the creation a super-hydrophobic surface on 304 stainless steel in medical applications", Surfaces and Interfaces, 2017, 8, 219–224.

[7] Chipatecua, Y. L., Olaya, J. J., Arias, D. F., Y.L. Chipatecua a, J.J. Olaya a, D. F. A., Chipatecua, Y. L., Olaya, J. J., and Arias, D. F., "Corrosion behaviour of CrN/Cr multilayers on stainless steel deposited by unbalanced magnetron sputtering", Vacuum, 2012, 86, 1393–1401.

[8] Bernoulli, D., Cao, S. C., Lu, J., and Dao, M., "Enhanced repeated frictional sliding properties in 304 stainless steel with a gradient nanostructured surface", Surf. Coatings Technol., 2018, 339, 14–19.

[9] Jin, X., Gao, L., Liu, E., Yu, F., Shu, X., and Wang, H., "Microstructure, corrosion and tribological and antibacterial properties of Ti–Cu coated stainless steel", J. Mech. Behav. Biomed. Mater., 2015, 50, 23–32.

[10] Mohamadian Samim, P., Fattah-Alhosseini, A., Elmkhah, H., and Imantalab, O., "Structure and corrosion behavior of ZrN/CrN nano-multilayer coating deposited on AISI 304 stainless steel by CAE-PVD technique", J. Asian Ceram. Soc., 2020, 8, 460–469.

[11] Babaei, K., Fattah-alhosseini, A., Elmkhah, H., Imantalab, O., and Ghomi, H., "Studying the in vitro corrosion response of nanostructured TaN coatings in Hank's physiological solution", Int. J. Appl. Ceram. Technol., 2021, 1–12.

[12] Babaei, K., Fattah-alhosseini, A., Elmkhah, H., and Ghomi, H., "Surface characterization and electrochemical properties of tantalum nitride (TaN) nanostructured coatings produced by reactive DC magnetron sputtering", Surfaces and Interfaces, 2020, 21, 100685.

[13] Mansoor, N. S., Fattah-alhosseini, A., Elmkhah, H., and Shishehian, A., "Electrochemical behavior of TiN, CrN and TiN/CrN nanostructured coatings on the nickel-chromium alloy used in dental fixed prosthesis", J. Asian Ceram. Soc., 2020, 8, 694–710.

[14] Guo, Z., Ma, D., Zhang, X., Li, J., and Feng, J., "Preparation and toughening of a-CuZr/c-ZrN nano-multilayer hard coatings", Appl. Surf. Sci., 2019, 483, 432–441.

[15] Maksakova, O. V., Simoẽs, S., Pogrebnjak, A. D., Bondar, O. V., Kravchenko, Y. O., Koltunowicz, T. N., and Shaimardanov, Z. K., "Multilayered ZrN/CrN coatings with enhanced thermal and mechanical properties", J. Alloys Compd., 2019, 776,




[ DOI: 10.22068/ijmse.2615 ]

679–690.

[16] Abdeen, D., El Hachach, M., Koc, M., and Atieh, M., "A Review on the Corrosion Behaviour of Nanocoatings on Metallic Substrates", Materials (Basel)., 2019, 12, 210.

[17] Kameneva, A. and Kichigin, V., "Corrosion, wear, and friction behavior of a number of multilayer two-, three- and multicomponent nitride coatings on different substrates, depending on the phase and elemental composition gradient", Appl. Surf. Sci., 2019, 489, 165–174.

[18] Maksakova, O., Simoẽs, S., Pogrebnjak, A., Bondar, O., Kravchenko, Y., Beresnev, V., and Erdybaeva, N., "The influence of deposition conditions and bilayer thickness on physical-mechanical properties of CA-PVD multilayer ZrN/CrN coatings", Mater. Charact., 2018, 140, 189–196.

[19] Pei, C., Deng, L., Liu, H., He, Z., Xiang, C., Zhang, S., and Sun, D., "Corrosion inhibition behaviors of ZrNx thin films with varied N vacancy concentration", Vacuum, 2019, 162, 28–38.

[20] Bemporad, E., Pecchio, C., De Rossi, S., and Carassiti, F., "Characterisation and wear properties of industrially produced nanoscaled CrN/NbN multilayer coating", Surf. Coatings Technol., 2004, 188, 319–330.

[21] Zhang, Z. G., Rapaud, O., Bonasso, N., Mercs, D., Dong, C., and Coddet, C., "Microstructures and corrosion behaviors of Zr modified CrN coatings deposited by DC magnetron sputtering", Vacuum, 2008, 82, 1332–1336.

[22] Sun, P. L., Hsu, C. H., Liu, S. H., Su, C. Y., and Lin, C. K., "Analysis on microstructure and characteristics of TiAlN/CrN nano-multilayer films deposited by cathodic arc deposition", Thin Solid Films, 2010, 518, 7519–7522.

[23] Cai, F., Yang, Q., Huang, X., and Wei, R., "Microstructure and corrosion behavior of CrN and CrSiCN coatings", J. Mater. Eng. Perform., 2010, 19, 721–727.

[24] Guan, X., Wang, Y., Zhang, G., Jiang, X., Wang, L., and Xue, Q., "Microstructures and properties of Zr/CrN multilayer coatings fabricated by multi-arc ion plating", Tribol. Int., 2017, 106, 78–87.

[25] Warcholiński, B., Gilewicz, A., Kukliński, Z., and Myśliński, P., "Arc-evaporated CrN, CrN and CrCN coatings", Vacuum, 2008, 83, 715–718.

[26] Warcholinski, B., Gilewicz, A., Kuklinski, Z., and Myslinski, P., "Hard CrCN/CrN multilayer coatings for tribological applications", Surf. Coatings Technol., 2010, 204, 2289–2293.

[27] Kravchenko, Y. O., Coy, L. E., Peplińska, B., Iatsunskyi, I., Załęski, K., Kempiński, M., Beresnev, V. M., Konarski, P., Jurga, S., and Pogrebnjak, A. D., "Nano-multilayered coatings of (TiAlSiY)N/MeN (Me=Mo, Cr and Zr): Influence of composition of the alternating layer on their structural and mechanical properties", J. Alloys Compd., 2018, 767, 483–495.

[28] Huang, J.-H., Kuo, K.-L., and Yu, G.-P., "Oxidation behavior and corrosion resistance of vacuum annealed ZrN-coated stainless steel", Surf. Coatings Technol., 2019, 358, 308–319.

[29] Wang, D., Hu, M., Jiang, D., Fu, Y., Wang, Q., Yang, J., Sun, J., and Weng, L., "The improved corrosion resistance of sputtered CrN thin films with Cr-ion bombardment layer by layer", Vacuum, 2017, 143, 329–335.

[30] Chim, Y. C., Ding, X. Z., Zeng, X. T., and Zhang, S., "Oxidation resistance of TiN, CrN, TiAlN and CrAlN coatings deposited by lateral rotating cathode arc", Thin Solid Films, 2009, 517, 4845–4849.

[31] Wiecinski, P., Smolik, J., Garbacz, H., and Kurzydlowski, K. J., "Microstructure and mechanical properties of nanostructure multilayer CrN/Cr coatings on titanium alloy", Thin Solid Films, 2011, 519, 4069–4073.

[32] Nam, N. D., Jo, D. S., Kim, J. G., Yoon, D. H., "Corrosion protection of CrN/TiN multi-coating for bipolar plate of polymer electrolyte membrane fuel cell", Thin Solid Films, 2011, 519, 6787-6791.

[33] Barshilia, H. C., Prakash, M. S., Poojari, A., and Rajam, K. S., "Corrosion behavior of nanolayered TiN/NbN multilayer coatings prepared by reactive direct current magnetron sputtering process", Thin Solid Films, 2004, 460, 133–142.



[ DOI: 10.22068/ijmse.2615 ]

[34] Feng, K., Li, Z., Lu, F., Huang, J., Cai, X., and Wu, Y., "Corrosion resistance and electrical properties of carbon/chromium-titanium- nitride multilayer coatings on stainless steel", J. Power Sources, 2014, 249, 299–305.
[35] Li, H., Zhang, C., Liu, C., and Huang, M., "Improvement in corrosion resistance of CrN coatings", Surf. Coatings Technol., 2019, 365, 158–163.
[36] Cai, Q., Li, S., Pu, J., Bai, X., Wang, H., Cai, Z., and Wang, X., "Corrosion resistance and antifouling activities of silver-doped CrN coatings deposited by magnetron sputtering", Surf. Coatings Technol., 2018, 354, 194–202.
[37] Ezirmik, V., Senel, E., Kazmanli, K., Erdemir, A., and Ürgen, M., "Effect of copper addition on the temperature dependent reciprocating wear behaviour of CrN coatings", Surf. Coatings Technol., 2007, 202, 866–870.
[38] Zhang, X., Huang, X., Ma, Y., Lin, N., Fan, A., and Tang, B., "Bactericidal behavior of Cu-containing stainless steel surfaces", Appl. Surf. Sci., 2012, 258, 10058–10063.
[39] Zhang, E., Wang, X., Chen, M., and Hou, B., "Effect of the existing form of Cu element on the mechanical properties, bio-corrosion and antibacterial properties of Ti-Cu alloys for biomedical application", Mater. Sci. Eng. C, 2016, 69, 1210–1221.
[40] Sahib Mansoor, N., Fattah-alhosseini, A., Shishehian, A., and Elmkahah, H., "Tribological properties of different types of coating materials deposited by cathodic arc-evaporation method on Ni-Cr dental alloy", Mater. Res. Express, 2019, 6, 056421.
[41] Weber, F. R., Fontaine, F., Scheib, M., and Bock, W., "Cathodic arc evaporation of (Ti, Al)N coatings and (Ti, Al)N/TiN multilayer-coatings-correlation between lifetime of coated cutting tools, structural and mechanical film properties", Surf. Coatings Technol., 2004, 177, 227–232.
[42] Teppernegg, T., Czettl, C., Michotte, C., and Mitterer, C., "Arc evaporated Ti-Al-N/Cr-Al-N multilayer coating systems for cutting applications", Int. J. Refract. Met. Hard Mater., 2018, 72, 83–88.
[43] Li, J., Zheng, H., Sinkovits, T., Hee, A. C., and Zhao, Y., "Mono- and multiple TiN(/Ti) coating adhesion mechanism on a Ti-13Nb-13Zr alloy", Appl. Surf. Sci., 2015, 355, 502–508.
[44] Sanchette, F., Ducros, C., Schmitt, T., Steyer, P., and Billard, A., "Nanostructured hard coatings deposited by cathodic arc deposition: From concepts to applications", Surf. Coatings Technol., 2011, 205, 5444–5453.
[45] Braic, M., Braic, V., Balaceanu, M., Zoita, C. N., Kiss, A., Vladescu, A., Popescu, A., and Ripeanu, R., "Structure and properties of Zr/ZrCN coatings deposited by cathodic arc method", Mater. Chem. Phys., 2011, 126, 818–825.
[46] Lomello, F., Sanchette, F., Schuster, F., Tabarant, M., and Billard, A., "Influence of bias voltage on properties of AlCrN coatings prepared by cathodic arc deposition", Surf. Coatings Technol., 2013, 224, 77–81.
[47] Jokar, K., Elmkhah, H., Fattah-alhosseini, A., Babaei, K., and Zolriasatein, A., "Comparison of the wear and corrosion behavior between CrN and AlCrN coatings deposited by Arc-PVD method", Mater. Res. Express, 2019, 6, 116426.
[48] Gilewicz, A., Chmielewska, P., Murzynski, D., Dobruchowska, E., and Warcholinski, B., "Corrosion resistance of CrN and CrCN/CrN coatings deposited using cathodic arc evaporation in Ringer's and Hank's solutions", Surf. Coatings Technol., 2016, 299, 7–14.
[49] Rtimi, S., Dionysiou, D. D., Pillai, S. C., and Kiwi, J., "Advances in catalytic/photocatalytic bacterial inactivation by nano Ag and Cu coated surfaces and medical devices", Appl. Catal. B Environ., 2019, 240, 291–318.
[50] Jönsson, B. and Hogmark, S., "Hardness measurements of thin films", Thin Solid Films, 1984, 114, 257–269.
[51] Vidakis, N., Antoniadis, A., and Bilalis, N., "The VDI 3198 indentation test evaluation of a reliable qualitative control for layered compounds", J. Mater. Process. Technol., 2003, 143, 481–485.
[52] Mohamadian Samim, P., Fattah-alhosseini, A., Elmkhah, H., and Imantalab, O., "A study on the corrosion resistance of



[ DOI: 10.22068/ijmse.2615 ]

ZrN/CrN multilayer nanostructured coating applied on AISI 304 stainless steel using Arc-PVD method in 3.5 wt% NaCl solution", Mater. Res. Express, 2019, 6, 126426.

[53] Mansoor, N. S., Fattah-alhosseini, A., Elmkhah, H., and Shishehian, A., "Assessment of Ion Release for Ni-Cr Dental Alloy with Monolithic and Multilayer Coatings in Different pH Level", Surfaces and Interfaces, 2021, 22, 100904.

[54] Song, G.-H., Yang, X.-P., Xiong, G.-L., Lou, Z., and Chen, L.-J., "The corrosive behavior of Cr/CrN multilayer coatings with different modulation periods", Vacuum, 2013, 89, 136–141.

[55] Kim, Y. J., Byun, T. J., Lee, H. Y., and Han, J. G., "Effect of bilayer period on CrN/Cu nanoscale multilayer thin films", Surf. Coatings Technol., 2008, 202, 5508–5511.

[56] Ma, F., Li, J., Zeng, Z., and Gao, Y., "Tribocorrosion behavior in artificial seawater and anti-microbiologically influenced corrosion properties of TiSiN-Cu coating on F690 steel", J. Mater. Sci. Technol., 2019, 35, 448–459.

[57] Polychronopoulou, K., Demas, N. G., Gibson, P. N., Rebholz, C., and Polycarpou, A. A., "Effect of Cu Content on the Structure, and Performance of Substoichiometric Cr–N Coatings", Tribol. Lett., 2010, 38, 57–68.

[58] Baker, M. A., Kench, P. J., Tsotsos, C., Gibson, P. N., Leyland, A., and Matthews, A., "Investigation of the nanostructure and wear properties of physical vapor deposited CrCuN nanocomposite coatings", J. Vac. Sci. Technol. A Vacuum, Surfaces, Film., 2005, 23, 423–433.

[59] Postolnyi, B. O., Beresnev, V. M., Abadias, G., Bondar, O. V., Rebouta, L., Araujo, J. P., and Pogrebnjak, A. D., "Multilayer design of CrN/MoN protective coatings for enhanced hardness and toughness", J. Alloys Compd., 2017, 725, 1188–1198.

[60] Kuppusami, P., Elangovan, T., Murugesan, S., Thirumurugesan, R., Khan, S., George, R. P., Ramaseshan, R., Divakar, R., Mohandas, E., and Mangalaraj, D., "Microstructural, nanomechanical and antibacterial properties of magnetron sputtered nanocomposite thin films of CrN/Cu", Surf. Eng., 2012, 28, 134–140.

[61] Sahami-Nejad, M., Lashgari, H. R., Zangeneh, S., and Kong, C., "Determination of residual stress on TIG-treated surface via nanoindentation technique in Co-Cr-Mo-C alloy", Surf. Coatings Technol., 2019, 380, 125020.

[62] Fattah-alhosseini, A., Vakili-Azghandi, M., Sheikhi, M., and Keshavarz, M. K., "Passive and electrochemical response of friction stir processed pure Titanium", J. Alloys Compd., 2017, 704, 499–508.

[63] Samim, P. M., Fattah-alhosseini, A., Elmkhah, H., Imantalab, O., and Nouri, M., "A study on comparing surface characterization and electrochemical properties of single-layer CrN coating with nanostructured multilayer ZrN/CrN coating in 3.5 wt.% NaCl solution", Surfaces and Interfaces, 2020, 21, 100721.

[64] Olaya, J. J., Rodil, S. E., Muhl, S., and Sánchez, E., "Comparative study of chromium nitride coatings deposited by unbalanced and balanced magnetron sputtering", Thin Solid Films, 2005, 474, 119–126.

[65] Ibrahim, M. A., Korablov, S., and Yoshimura, M., "Corrosion of stainless steel coated with TiN, (TiAl)N and CrN in aqueous environments", Corros. Sci., 2002, 44, 815–828.

[66] Imantalab, O. and Fattah-alhosseini, A., "Electrochemical and Passive Behaviors of Pure Copper Fabricated by Accumulative Roll-Bonding (ARB) Process", J. Mater. Eng. Perform., 2015, 24, 2579–2585.

[67] Fattah-alhosseini, A. and Imantalab, O., "Passivation Behavior of Ultrafine-Grained Pure Copper Fabricated by Accumulative Roll Bonding (ARB) Process", Metall. Mater. Trans. A, 2016, 47, 572–580.

[68] Fattah-Alhosseini, A., Attarzadeh, F. R., and Vakili-Azghandi, M., "Effect of Multi-pass Friction Stir Processing on the Electrochemical and Corrosion Behavior of Pure Titanium in Strongly Acidic Solutions", Metall. Mater. Trans. A, 2017, 48, 403–411.

[69] Fattah-alhosseini, A., Yazdani Khan, H.,



[ DOI: 10.22068/ijmse.2615 ]

and Heidarpour, A., "Comparison of anti-corrosive properties between hot alkaline nitrate blackening and hydrothermal blackening routes", J. Alloys Compd., 2016, 676, 474–480.

[70] Schönleber, M., Klotz, D., and Ivers-Tiffée, E., "A Method for Improving the Robustness of linear Kramers-Kronig Validity Tests", Electrochim. Acta, 2014, 131, 20–27.

[71] Fajardo, S., Bastidas, D. M., Criado, M., and Bastidas, J. M., "Electrochemical study on the corrosion behaviour of a new low-nickel stainless steel in carbonated alkaline solution in the presence of chlorides", Electrochim. Acta, 2014, 129, 160–170.

[72] Elmkhah, H., Abdollah-zadeh, A., Mahboubi, F., Rouhaghdam, A. R. S., and Fattah-alhosseini, A., "Correlation between the duty cycle and the surface characteristics for the nanostructured titanium aluminum nitride coating deposited by pulsed-DC PACVD technique", J. Alloys Compd., 2017, 711, 530–540.

[73] Lotfi-khojasteh, E., Sahebazamani, M., Elmkhah, H., Nouri, M., Imantalab, O., and Fattah-alhosseini, A., "A study of the electrochemical and tribological properties of TiN/CrN nano-layer coating deposited on carburized-H13 hot-work steel by Arc-PVD technique", J. Asian Ceram. Soc., 2021, 9, 247–259.

[74] Elmkhah, H., Fattah-alhosseini, A., Babaei, K., Abdollah-Zadeh, A., and Mahboubi, F., "Correlation between the Al content and corrosion resistance of TiAlN coatings applied using a PACVD technique", J. Asian Ceram. Soc., 2020, 8, 72–80.

[75] Vakili-Azghandi, M. and Fattah-alhosseini, A., "Effects of Duty Cycle, Current Frequency, and Current Density on Corrosion Behavior of the Plasma Electrolytic Oxidation Coatings on 6061 Al Alloy in Artificial Seawater", Metall. Mater. Trans. A, 2017, 48, 4681–4692.

[76] Rosalbino, F., Angelini, E., Macciò, D., Saccone, A., and Delfino, S., "Application of EIS to assess the effect of rare earths small addition on the corrosion behaviour of Zn–5% Al (Galfan) alloy in neutral aerated sodium chloride solution", Electrochim. Acta, 2009, 54, 1204–1209.

[77] Fattah-alhosseini, A., Gashti, S. O., and Keshavarz, M. K., "Effect of Film Formation Potential on Passive Behavior of Ultra-Fine-Grained 1050 Al Alloy Fabricated via ARB Process", J. Mater. Eng. Perform., 2016, 25, 1683–1689.

[78] Ebrahimi, A., Esfahani, H., Fattah-alhosseini, A., and Imantalab, O., "In-vitro electrochemical study of $TiB/TiB_2$ composite coating on titanium in Ringer's solution", J. Alloys Compd., 2018, 765, 826–834.

[79] Nam, N. D., Kim, M. J., Jo, D. S., Kim, J. G., and Yoon, D. H., "Corrosion protection of Ti/TiN, Cr/TiN, Ti/CrN, and Cr/CrN multi-coatings in simulated proton exchange membrane fuel cell environment", Thin Solid Films, 2013, 545, 380–384.

[80] Wang, H. ., Stack, M. ., Lyon, S. ., Hovsepian, P., and Münz, W.-D., "The corrosion behaviour of macroparticle defects in arc bond-sputtered CrN/NbN superlattice coatings", Surf. Coatings Technol., 2000, 126, 279–287.

[81] Postelnyk, H., Sobol, O., Chocholaty, O., and Knyazev, S., "Structure and Corrosion Resistance of Vacuum-Arc Multi-period CrN/Cu Coatings", Advances in Design, Simulation and Manufacturing III. DSMIE 2020. Lecture Notes in Mechanical Engineering., 2020, 532–541.

[82] Liao, K.-H., Ou, K.-L., Cheng, H.-C., Lin, C.-T., and Peng, P.-W., "Effect of silver on antibacterial properties of stainless steel", Appl. Surf. Sci., 2010, 256, 3642–3646.

[83] Huang, C.-F., Chiang, H.-J., Lan, W.-C., Chou, H.-H., Ou, K.-L., and Yu, C.-H., "Development of silver-containing austenite antibacterial stainless steels for biomedical applications Part I: microstructure characteristics, mechanical properties and antibacterial mechanisms", Biofouling, 2011, 27, 449–457.

[84] Elangovan, T., George, R. P., Kuppusami, P., Mangalaraj, D., Bera, S., Mohandas, E., and Kim, D.-E., "Development of a CrN/Cu nanocomposite coating on titanium-modified stainless steel for antibacterial activity against Pseudomonas aeruginosa", Biofouling, 2012, 28, 779–787.



[ DOI: 10.22068/ijmse.2615 ]